19th Brazilian Congress of Thermal Sciences and Engineering
November 6th–10th, 2022, Bento Gonçalves - RS - Brazil

ENC-2022-0157
Analysis of the impacts caused by the insertion of leading-edge tubercles over a Francis turbine runner

Henrique Matos Campos
Leandro Oliveira Salviano
Aluisio Viais Pantaleão
Department of Mechanical Engineering, School of Engineering, São Paulo State University (Unesp), Brazil
hmatoscampos@gmail.com, leandro.salviano@unesp.br, aluisio.pantaleao@unesp.br

Abstract.
To keep the development of the hydroelectricity sector in Brazil, one of the alternatives found in the literature is the use of passive devices for turbomachinery, such as the insertion of leading-edge tubercles. Until now, the effects of the tubercles insertion in hydraulic turbines are unknown. With this study, we seek to solve this gap in the literature by developing a numerical methodology using the software Ansys CFX to verify and quantify the impacts of the insertion of the device over the runner of the Francis-99 turbine. Also, we tested the effects of the main tubercles parameters on the turbine performance, which we did by testing six different configurations of the device, considering variations in their amplitude and wavelength. As a result, we obtained minor gains in torque generation, up to 0.356%, being the positive results found for the turbine operating at its best efficiency point or under high load conditions. Analyzing the effects of the tubercle parameters on the turbine performance, we verified that the tubercles with higher amplitudes provided the highest gains in torque generation, and the wavelength variation provided minimal impacts on the device.

Keywords: *CFD; CFX; Francis turbines; Leading-edge tubercles; Francis-99*

1. INTRODUCTION

In Brazil, hydroelectricity is the main source of electricity generation, being responsible for more than 60% of the electric energy of the country, as presented by Ministério de Minas e Energia (MME) and Empresa de Pesquisa Energética (EPE) (2020). However, according to Ministério de Minas e Energia (MME) and Empresa de Pesquisa Energética (EPE) (2020) previsions, the hydroelectricity participation in the Brasilian electrical matrix will shrink in the nearing future due to the difficulties found in the construction of new power plants and the growth of other renewable sources of energy. Despite the limitations found for the growth of the hydroelectricity sector, there are still some viable ways to keep the development of this sector, such as the construction of small hydroelectric power plants and the modernization of the existing projects.

The modernization of hydroelectric power plants can be done by appling passive flow control methods for turbo machinery in the turbine project, such as the use of cavitation-bubble generators (Kadivar *et al.* (2018), and Kadivar *et al.* (2019)), slots (Liu *et al.* (2020)), barriers (Chen *et al.* (2017)), and leading-edge tubercles (Gruber *et al.* (2011), Shi *et al.* (2016), (Zhang and Wu (2012), Abate and Mavris (2017) and Zhang *et al.* (2022)), being the latter one of the alternatives that stands out in literature.

The leading-edge tubercles are a bio-inspired device that takes the humpback whale (*Megaptera novaeangliae*) flippers as inspiration. According to Fish and Battle (1995), the existence of the large tubercles in the humpback whale flippers' leading-edge, like the ones shown in Figure 1, provides the reduction of the drag and the postponing of the stall over the flipper, which consequently improves the animal hydrodynamic performance.

The tubercle's impacts occur due to their influence on the flow around the humpback whales' flippers. According to Abate and Mavris (2017), these structures redirect the fluid flow, causing its acceleration and creating counter-rotating vortices in the flow. The generated vortices amplify the momentum exchange in the boundary layer, causing the delay in the boundary layer separation, which provides the gains verified in the animal flippers. As presented by Gruber *et al.* (2011), the behavior of the flow around the tubercles is similar to the one found in vortex generators added to the leading edge.

Figure 1: Tubercles found in the humpback whales' flippers. Available from: https://asknature.org/strategy/flippers-provide-lift-reduce-drag/

In the literature applications of the leading-edge tubercles on tidal turbines (Gruber *et al.* (2011), and Shi *et al.* (2016)) and on eolic turbines (Zhang and Wu (2012), Abate and Mavris (2017) and Zhang *et al.* (2022)) have already been done. However, until now, no application of these structures in hydraulic turbines has been found.

For tidal turbines Gruber *et al.* (2011) and Shi *et al.* (2016) obtained similar results in their studies. By analyzing the insertion of leading-edge tubercles in a tidal turbine with a NACA 63_3-618 hydrofoil cross-section, Gruber *et al.* (2011) verified that the tubercles increased the pressure coefficient between 15% and 85%, being the gains verified especially at lower flow velocities. By testing leading-edge tubercles on a turbine with NREL S814 hydrofoil cross-section, Shi *et al.* (2016) also concluded that the impact of the device occurs mainly at low flow velocities, where the generated torque increases around 40% for a 0° pitch angle. While at higher flow velocities, the increase was between 15% to 20%.

For NREL phase-VI wind turbines, Zhang and Wu (2012) obtained that the insertion of leading-edge tubercles increased the torque generation in high flow velocities, up to 24.8%, but reduced it, up to 24.7%, in low flow velocities. For the same wind turbine geometry, Abate and Mavris (2017) obtained similar conclusions for the behavior of the torque generation with the velocity variation, only diverging that Abate and Mavris (2017) verified that the tubercles insertion provided a maximum increase of 5% in torque generation. Studying vertical axis wind turbines based on the NACA 0021 cross-section, Zhang *et al.* (2022) verified that the addition of the leading-edge tubercles provided up to 7.35% more torque generation for all the range of velocities tested.

As we can see for wind and tidal turbines, the insertion of leading-edge tubercles improved the shaft torque generation for at least some of the turbines' operation points. Due to that, during this study, we decided to verify if the tubercles insertion could provide the same gains for hydraulic turbines. Also, we decided to test how the main structural parameters of the leading-edge tubercles affect the hydraulic turbine performance.

To achieve our objectives, during the study, we tested the impacts of the leading-edge tubercles insertion in the reference geometry of the Francis-99 turbine provided by the homonym workshop[1] using a numerical methodology based on the CFD code Ansys CFX.

2. METHODOLOGY

2.1 Analized geometry, flow conditions and mathematical model

To develop our analysis, we used the Francis-99 turbine as reference geometry. This turbine is a scaled model of the Tokke power plant Francis turbines, provided by the NTNU (Norwegian University of Science and Technology) for the Francis-99 workshop series. Also, during each workshop edition, the NTNU provides the turbine operating conditions, experimental data for validation, and benchmarking meshes.

For our analysis, we based our study on the second Francis-99 workshop. In this edition, the NTNU provided data for three operating three operation conditions of the turbine; part load (PL), best efficiency point (BEP), and high load (HL); being these operation points detailed in Table 1.

For the second Francis-99 workshop, the NTNU used the definitions of the net head (H) and hydraulic efficiency (η), respectively determined in equations 1 and 2.

$$H = \frac{p_{inlet} - p_{outlet}}{\rho g} + \frac{|\vec{v}_{inlet}|^2 - |\vec{v}_{outlet}|^2}{2g} + \Delta z \tag{1}$$

[1] Details presented by NTNU at https://www.ntnu.edu/nvks/francis-99.

$$\eta = \frac{2\pi\omega T}{\rho Q g H} \tag{2}$$

Being in Equations 1 and 2: p the pressure, ρ the water density, g the gravity, v the flow velocity, Δz the height difference between inlet and outlet pressure measurement, ω the runner angular speed, T the torque to the generator, and Q the turbine discharge.

For the Francis-99 turbine, the height difference considered was 1.0715 m. The fluid flow velocity was calculated by dividing the discharge by the cross-sectional reference area. For the turbine, the inlet and outlet cross-sectional reference areas were respectively 0.0962 m^2 and 0.236 m^2.

Table 1: Francis-99 operation conditions presented by the NTNU during the second Francis-99 workshop[2].

Parameter	**PL**	**BEP**	**HL**	**Uncertainty**
Guide vane angle (°)	6.72	9.84	12.43	$\pm 0.04°$
Net head (m)	11.87	11.94	11.88	$\pm 0.011\%$
Discharge (m^3/s)	0.13962	0.19959	0.24246	$\pm 0.01\%$
Torque to the generator (Nm)	416.39	616.13	740.54	$\pm 0.03\%$
Friction torque (Nm)	4.40	4.52	3.85	$\pm 1.5\%$
Runner angular speed (rpm)	332.84	332.59	332.59	$\pm 0.05\%$
Casing inlet pressure (kPa)	218.08	215.57	212.38	$\pm 0.047\%$
Draft tube outlet pressure (kPa)	113.17	113.13	109.59	$\pm 0.001\%$
Water density (kg/m^3)	999.8	999.8	999.8	$\pm 0.01\%$
Kinematic viscosity (m^2/s)	$9.57 \cdot 10^{-7}$	$9.57 \cdot 10^{-7}$	$9.57 \cdot 10^{-7}$	-
Gravity (m/s^2)	9.82	9.82	9.82	-
Hydraulic efficiency (%)	90.13	92.39	91.71	$\pm 0.14\%$

To develop our mathematical model for the turbine, we used as base Trivedi *et al.* (2013) study, one of the references for the second version of the workshop. In this case, according to Trivedi *et al.* (2013), the fluid is considered Newtonian, and the fluid flow is incompressible and turbulent. The second version of the workshop Francis-99 and Trivedi *et al.* (2013) analyze the Francis-99 turbine operating in steady-state and transient conditions. However, to test the impacts of the leading-edge tubercles, we only considered steady-state flows.

With the adopted considerations, we needed to solve as governing equations the mass conservation and the momentum equation, respectively presented in equations 3 and 4. To model the turbulent effects, we adopted the RANS approach and used the RNG k-epsilon turbulence model, proposed by Yakhot *et al.* (1992), to solve the closure problem. Due to that, during the numerical simulations, along with the governing equations, we also solved the transport Equations for the turbulent kinetic energy (k) and the rate of dissipation of turbulence kinetic energy (ϵ), respectively shown in equations 5 and 6.

$$\nabla \cdot \vec{v} = 0 \tag{3}$$

$$\rho \nabla \cdot (\{\vec{v}\vec{v}\}) = -\nabla p + \nabla \cdot (\mu[\nabla(\vec{v}) + \nabla(\vec{v})^T]) + \rho\vec{g} - 2\rho(\vec{\omega} \times \vec{v}) - \rho[\vec{\omega} \times (\vec{\omega} \times \vec{r})] \tag{4}$$

$$\nabla \cdot (\vec{v}k) = \nabla \cdot \left(\left[\nu + \frac{\nu_t}{\sigma_k} \right] \nabla k \right) + \frac{P_k}{\rho} - \epsilon \tag{5}$$

$$\nabla \cdot (\vec{v}\epsilon) = \nabla \cdot \left(\left[\nu + \frac{\nu_t}{\sigma_\epsilon} \right] \nabla \epsilon \right) + (C_{\epsilon 1} - r)\frac{\epsilon}{\rho k} P_k - C_{\epsilon 2}\frac{\epsilon^2}{k} \tag{6}$$

Being in equations 4, 5 and 6: ν the kinematic viscosity, $\vec{r}$ the position vector, $\vec{\omega}$ the angular velocity, P_k a source term, r a function for the model and ν_t the turbulent viscosity. Also, in equations 5 and 6, σ_k, σ_e, $C_{\epsilon 1}$ are constants, being details of those provided by Yakhot *et al.* (1992).

Have to be noticed that to account the turbine rotational effects, the momentum equation, Equation 4, present in its formulation terms to account the Coriolis forces ($-2\rho(\vec{\omega} \times \vec{v})$) and the centrifugal forces ($-\rho[\vec{\omega} \times (\vec{\omega} \times \vec{r})]$).

2.2 Software and numerical methodology

We developed a numerical methodology based on the Finite Volume Method to solve the governing and transport equations. In this case, to do the domain discretization, we used Ansys Meshing[3], and to solve the equations, we used Ansys CFX[4], both software from Ansys 19.0 academic licensing.

[2] Experimental data provided by the NTNU in https://www.ntnu.edu/nvks/f99-test-case2.

For the analysis, we determined the computational domain following the Zhang *et al.* (2007) model. In this case, we analyzed the geometry presented in Figure 2. The studied geometry modeled the runner using one channel and the guide vane using two; and considered rotational periodicity to reproduce the complete set of these components, which we have done to reduce computational costs.

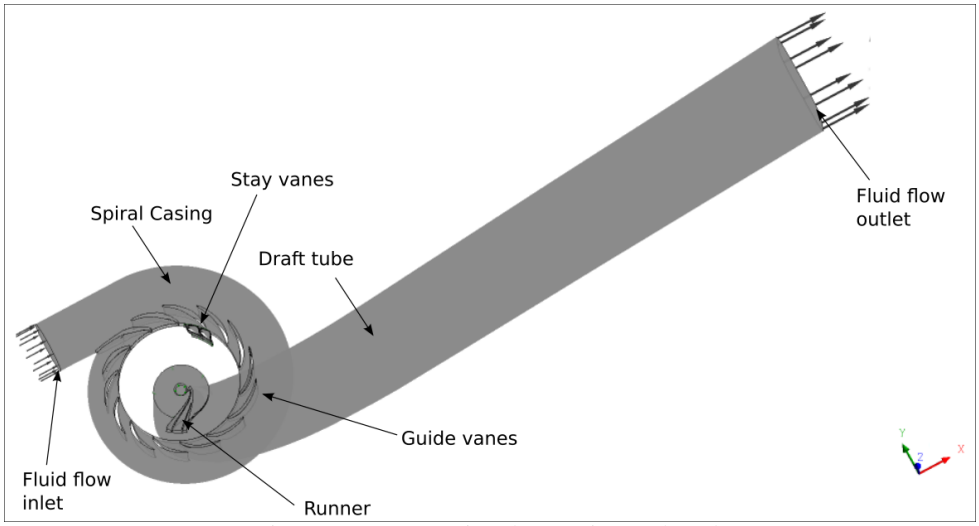

Figure 2: Computational Domain Analyzed.

Since the flow involves rotational effects to deal with these, we used the MRF ("Multiple Rotating Frame of reference") approach. Due to that, each of the turbine components was modeled independently and connected with the others using GGI (General Grid Interface) connection with the Frozen Rotor mixing model in their interfaces. The other boundary conditions adopted were the specification of the mass flow rate in the inlet, the specification of the uniform static pressure in the outlet, and the adoption of no-slip walls.

As numerical schemes, we adopted the High Resolution scheme for the discretization of the advection term and used the iterative method ILU (Incomplete Lower Upper) with the adoption of multigrid to solve the linear system of equations. During the study, we considered as convergence criteria an RMS error of 10^{-4} and a maximum of 5000 iterations.

2.3 Validation of the numerical methodology

Our first step to validate the developed numerical methodology was to simulate the flow with the benchmarking mesh provided by the workshop Francis-99[5] and compare the results found, presented in Table 2, with the experimental data presented in Table 1. By doing so, we verified an error between 9.41% to 11.69% for the net head (H), between 4.15% to 9.26% for the torque (T), and between 3.16% to 5.44% for the efficiency (η).

We observed that the higher errors for T and H occurred for the turbine operating in PL condition and the smaller ones for its operation in the HL. For η, the higher error occurs for the turbine operating in BEP and the smaller in PL. The highest error values found for H happen due to the simplifications done in the geometry and the fact that we calculated the inlet pressure rather than prescribed it. Comparing the errors found with other studies presented in the literature, like Dewan *et al.* (2017), Minakov *et al.* (2017), and Gavrilov *et al.* (2017), we observed that our results are compatible.

The second step of the numerical methodology validation was to generate our meshes and develop a grid convergence index (GCI) analysis. Since our focus was to modify the runner leading-edge, we kept the benchmarking meshes for all the other components and generated meshes only for the runner. Following the procedures proposed by Celik *et al.* (2008), we developed three meshes with a refinement factor (r) of at least 1.3, being mesh 1 with 7,980,023 elements, mesh 2 with 3,371,984 elements, and mesh 3 with 1,372,954 elements. After that, we performed the GCI analysis assuming T and η as the critical variables, being in Table 2 presented the results of the simulations of the generated meshes and in Table 3 exhibited the results of the GCI analysis.

As can be seen in Table 3, the GCI values are at most 0.509% for η and at most 0.217% for T. The maximum approximate relative error (e_a) and maximum extrapolated relative error (e_{ext}) are respectively 0.160% and 0.406%, being both verified for the efficiency in HL. Since the errors verified are low, and meshes presented an asymptotic convergence, during the study was possible to use the coarsest mesh (mesh 3) to represent the analyzed flow, ensuring an adequate result and an acceptable computational cost.

[3] Details about the software are provided by Ansys in https://www.ansys.com/products/meshing.

[4] Experimental data provided by the NTNU in Details about the software are provided by Ansys in https://www.ansys.com/products/fluids/ansys-cfx.

By comparing the results evaluated for the mesh 3 with the benchmarking mesh results, both presented in Table 2, we verified that the developed mesh exhibit smaller error values for the net head (e_H) and torque (e_T) in comparison with the benchmarking mesh, being observed a reduction between 2.384 to 2.559% for e_H, and between 3.138 to 3.206% for e_T. However, the generated mesh also presented a higher error for the efficiency (e_η), of at most 3.688%.

Table 2: Results obtained with the simulation of the benchmarking mesh and the meshes developed for GCI analysis.

	Oparating point	**H (m)**	**T (Nm)**	η **(%)**	$\mathbf{e_H}$ **(%)**	$\mathbf{e_T}$ **(%)**	$\mathbf{e_\eta}$ **(%)**
Benchmarking mesh	PL	13.258	455.94	87.283	11.693	9.258	3.159
	BEP	13.107	647.81	87.875	9.774	5.142	5.440
	HL	12.998	771.28	86.848	9.411	4.151	5.301
Mesh 3	PL	12.975	441.59	84.044	9.309	6.052	6.752
	BEP	12.838	628.35	84.447	7.521	1.983	9.128
	HL	12.694	748.04	83.727	6.852	1.013	8.705
Mesh 2	PL	12.976	441.67	84.051	9.318	6.071	6.745
	BEP	12.834	628.04	84.465	7.487	1.933	9.109
	HL	12.707	747.59	83.593	6.961	0.952	8.851
Mesh 1	PL	12.980	442.20	84.125	9.351	6.199	6.663
	BEP	12.831	628.47	84.544	7.462	2.003	9.024
	HL	12.698	747.92	83.690	6.886	0.997	8.745

Table 3: Results obtained with the simulation of the benchmarking mesh and the meshes developed for GCI analysis.

	PL		**BEP**		**HL**	
	$\mathbf{T\ (Nm)}$	η (%)	$\mathbf{T\ (Nm)}$	η (%)	$\mathbf{T\ (Nm)}$	η (%)
$\mathbf{r_{h,21}}$	1.333	1.333	1.333	1.333	1.333	1.333
$\mathbf{r_{h,32}}$	1.349	1.349	1.349	1.349	1.349	1.349
$\phi_{\mathbf{ext}}^{\mathbf{21}}$	441.574	84.043	629.174	84.441	749.242	84.068
$\phi_{\mathbf{ext}}^{\mathbf{32}}$	441.574	84.043	629.952	84.441	746.751	83.358
$\mathbf{e_a^{21}}$	0.018%	0.008%	0.049%	0.021%	0.060%	0.160%
$\mathbf{e_a^{32}}$	0.120%	0.088%	0.068%	0.094%	0.044%	0.116%
$\mathbf{e_{ext}^{21}}$	0.004%	0.001%	0.131%	0.007%	0.160%	0.406%
$\mathbf{e_{ext}^{32}}$	0.022%	0.009%	0.174%	0.028%	0.112%	0.282%
$\mathbf{GCI_{21}}$	0.004%	0.001%	0.164%	0.009%	0.201%	0.509%
$\mathbf{GCI_{32}}$	0.027%	0.012%	0.217%	0.035%	0.140%	0.351%

2.4 Insertion of the leading-edge tubercles

Since the developed methodology presented a good agreement with the experimental data and the literature results; and the generated meshes also were capable of representing the flow with small differences in comparison with the benchmarking mesh, the next step of the study was to insert the leading-edge tubercles in the Francis-99 turbine runner.

During the study, we tested six configurations of leading-edge tubercles, varying their geometry considering three values of amplitude (A), $A = 0.025b$, $0.05b$ and $0.11b$; and two values of wavelength (λ), $\lambda = 0.125b$ and $0.25b$, being all the studied geometries adapted from the models proposed by Johari *et al.* (2007). Figure 3a presents the definitions of A and λ for a blade, and Figure 3b exhibits one of the geometries of the Francis-99 runner with the leading-edge tubercles developed during the study.

3. RESULTS

By simulating the developed geometries, we obtained the results presented in Table 4 for the net head (H), torque (T), and efficiency (η). After that, we compared the results evaluated with the ones calculated for the mesh 3, presented in the Table 3, to estimate the difference caused by the tubercles insertion in the net head (ΔH) and in the torque (ΔT), being this comparison also presented in Table 4.

As can be seen in Table 4, the leading-edge tubercles insertion impacted more in the net head value, being the variation verified between 0.008% and 0.455%, which occurs due to the impact of the tubercles over the flow pressure. For most

[5] The benchmarking meshes are available at https://www.ntnu.edu/nvks/f99-test-case2.

of the tested configurations, the tubercles insertion increased the net head, excluding the configuration 8S, which reduced H between 0.039% and 0.070% in all the turbine operating points. The smaller variations, like 0.008%, occurs due to numerical erros and physically are equivalent to 0%.

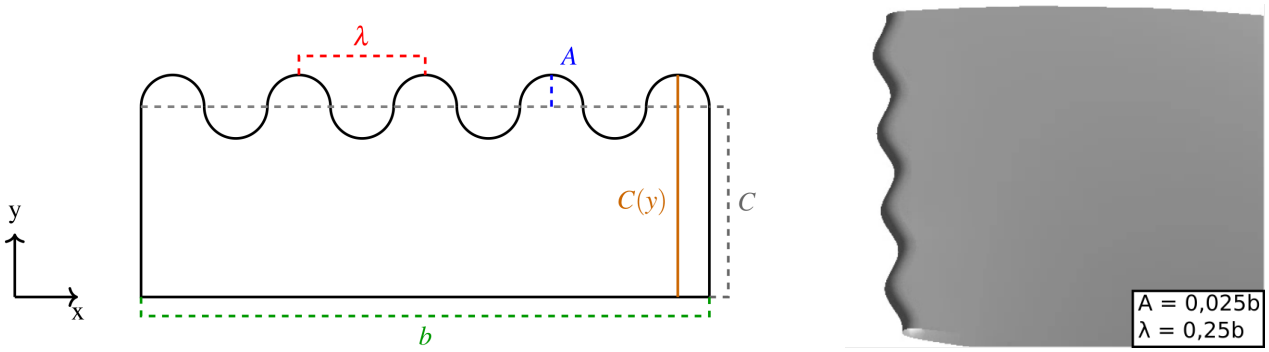

(a) Definition of tubercles amplitude (A) and wavelength (λ).

(b) Francis-99 leading edge with tubercles.

Figure 3: Details of the leading-edge tubercles definition and its use in Francis-99 runner.

Table 4: Results obtained with the simulation of the Francis-99 runner with the leading-edge tubercles configurations proposed by Johari *et al.* (2007).

Configuration	Operating point	H (m)	T (Nm)	η (%)	ΔH (%)	ΔT (%)
4S	PL	12.997	442.10	83.996	0.170	0.115
$\mathbf{A = 0.025b}$	BEP	12.853	629.10	84.482	0.117	0.119
$\lambda = \mathbf{0.250b}$	HL	12.703	748.57	83.725	0.071	0.071
8S	PL	12.970	441.18	83.993	-0.039	-0.093
$\mathbf{A = 0.025b}$	BEP	12.829	628.02	84.492	-0.070	-0.053
$\lambda = \mathbf{0.125b}$	HL	12.689	747.85	83.741	-0.039	-0.025
4M	PL	13.003	442.15	83.959	0.216	0.127
$\mathbf{A = 0.050b}$	BEP	12.847	629.22	84.531	0.070	0.138
$\lambda = \mathbf{0.250b}$	HL	12.695	748.48	83.766	0.008	0.059
8M	PL	13.007	441.89	83.895	0.247	0.068
$\mathbf{A = 0.050b}$	BEP	12.851	628.97	84.479	0.101	0.099
$\lambda = \mathbf{0.125b}$	HL	12.693	748.44	83.780	-0.008	0.053
4L	PL	13.028	442.29	83.830	0.408	0.159
$\mathbf{A = 0.110b}$	BEP	12.876	629.96	84.443	0.296	0.256
$\lambda = \mathbf{0.250b}$	HL	12.714	749.47	83.758	0.158	0.191
8L	PL	13.034	442.57	83.847	0.455	0.222
$\mathbf{A = 0.110b}$	BEP	12.893	630.59	84.419	0.428	0.356
$\lambda = \mathbf{0.125b}$	HL	12.729	750.36	83.754	0.276	0.310

For the torque the impacts verified with the tubercle insertion are lower than those found for H, as can be seen in Table 4. For T, the gains evaluated are up to 0.356%, being those observed in all the turbine operation points, excluding the configuration 8S that reduced T, between 0,025% and 0.093%.

Analyzing the effects of the amplitude variation in the tubercles' impact, we observed that the A elevation, increased T and H being the higher values of the parameters found, in all the turbine operating points, for the configurations L. By analyzing the other amplitudes tested, we verified that the configuration 4S presented minimal differences compared with configurations 4M and 8M. Being the last capable of providing slightly higher values of T and H in PL and BEP, while the first provided higher values in HL.

Comparing the efficiency values provided in Table 4, we plotted the curves of η with the discharge (Q), bein the result presented in Figure 4. As seen in the figure, in PL, the tubercle insertion caused a minimal reduction in the turbine efficiency. With Q increase, the tubercles provided minimal gains in the equipment efficiency, being the values of η slightly higher for configurations S and M in BEP and slightly higher for configurations M and L in HL.

As can be seen in Table 4, the effects of the wavelength variation weren't so significant, in comparison with the ones caused by the amplitude variation, for the tubercles' performance. When compared, configurations 4 and 8 presented similar results for all the tested configurations for H, T, and η, being the only significant difference observed between configurations 4S and 8S, which occurs due to the different behavior verified for the last configuration.

Also can be seen in Table 4 and Figure 4 that the leading-edge tubercles have their impacts reduced for H and η with the increase of the discharge, being the higher differences compared with the original runner geometry, observed in PL, and the lower observed in HL. For T, the tubercle insertion provided higher gains in BEP, which is an attraction to use the device due to the turbine being projected to operate at this operating point.

To develop a further study, we compared the Thoma number for the turbine with the plant Thoma number, following the methodology proposed by Celebioglu *et al.* (2017), to determine regions where the turbine operation is free of cavitation. The result of this comparison between the configuration 4L and the original runner is presented in Figure 5. Also, to verify the impacts of the leading-edge tubercles in the boundary layer, we analyzed the vorticity field around the blade, in Figure 6 is presented the results of this analysis for two sections of the 4L and original runner geometry.

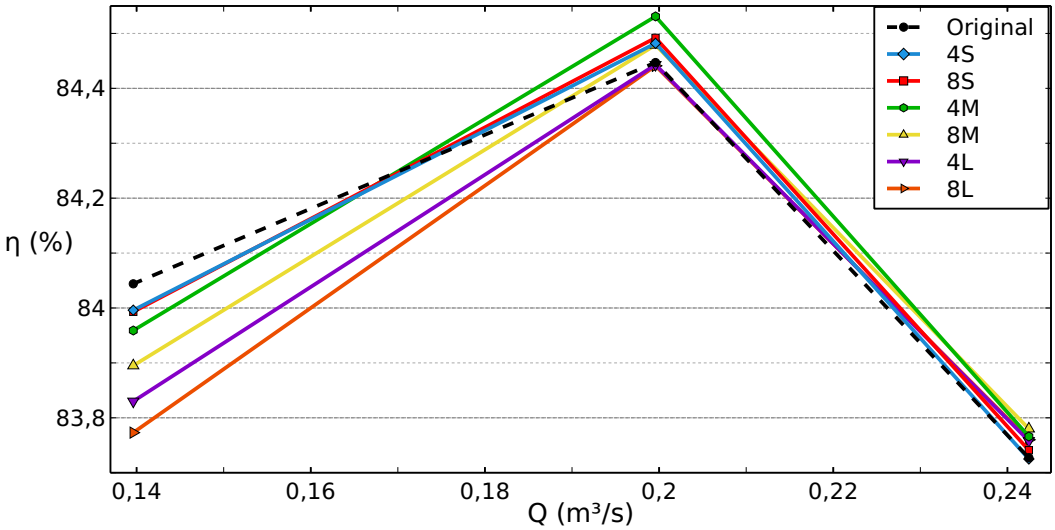

Figure 4: Behavior of the turbine efficiency (η) with the fluid flow discharge (Q).

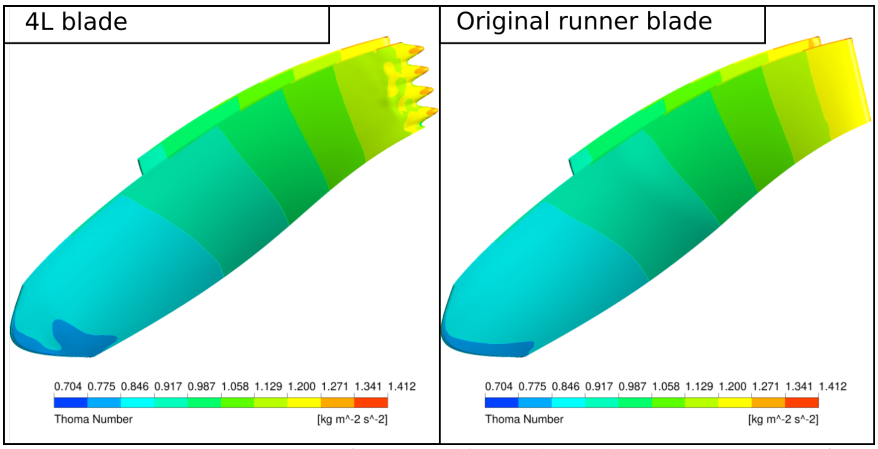

Figure 5: Comparison between the Thoma number for the turbine and the plant Thoma number for the tubercle configuration 4L and the original runner.

As can be seen in Figure 5, for the Francis-99 runner, we didn't verify any cavitation occurrence in both the analyzed runner geometry. The insertion of the leading-edge tubercles provided higher Thoma numbers next to the tubercles' crest and lower values next to the throughs compared with the original runner. Another difference observed occurs next to the runner trailing-edge, where the geometry with the leading-edge tubercles presented growth in the area with low Thoma numbers. Despite these differences in Thoma number behavior, we didn't verify any significant impact in this parameter with the tubercle insertion.

Analyzing the vorticity field presented in Figure 6, we verified that the geometry with the leading-edge tubercles exhibits significant differences compared with the original runner geometry. For regions next to a crest, like in section 1, the boundary layer detachment was delayed compared with the original runner. However, next to tubercles throughs, like in section 2, the boundary layer detachment occurred early.

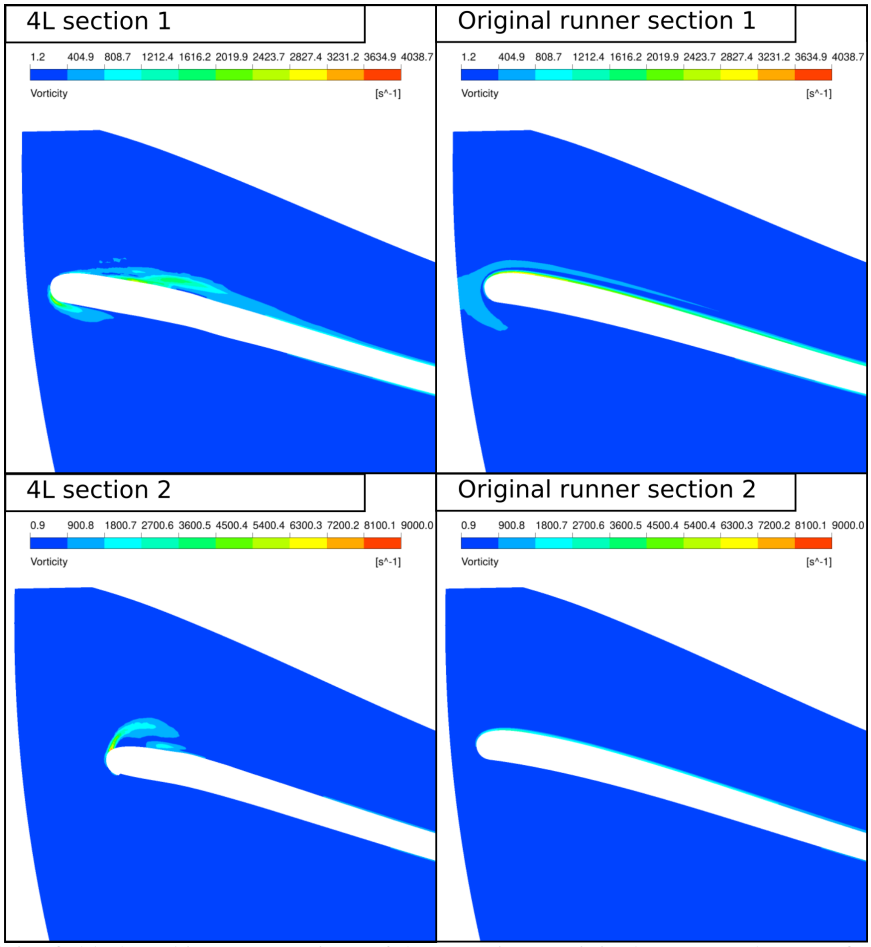

Figure 6: Vorticity field plotted in cross-sections of the Francis-99 original runner and 4L configuration runner.

4. CONCLUSIONS

Despite the simplifications done to reduce the computational costs, the numerical methodology developed during the study presented a good agreement with the experimental data and other literature studies, being the Ansys CFX capable of representing the physics involved in the flow over the Francis-99 turbine and the Ansys Meshing capable of generating adequate meshes of our computational domain. The higher errors found in the study occurred in the net head due to the inlet pressure didn't been specified but rather calculated.

Observing the data presented in Table 4 and Figure 4 can be noticed that the tubercles insertion provided small gains for torque, up to 0.356%, in BEP and HL, and caused small losses in PL. The considerably small impacts caused by the tubercles insertion possibly occur due to the Francis-99 turbine already being optimized. Since we verified that any modifications in its geometry caused minimal gains or led to negative impacts.

By analyzing the impacts caused by the parameters variation, we verified that the amplitude variation provided the higher neat head and torque values, being the configuration L the one with the highest values of both parameters in all the operating points. The wavelength variation provided minimal differences compared with the amplitude variation, except for the configuration 8S, which presented a different behavior from the other tested configurations.

Analyzing the flow around the turbine runner with the leading edge tubercles from the configuration 4L and comparing it with the flow field of the original runner geometry, we observed by comparing the Thoma number that the tubercles insertion provided minimal variations in the cavitation occurrence, as seen in the Figure 5. However, the device impacted significantly in boundary layer detachment, as can be seen with the analysis of the vorticity done in Figure 6.

To improve the understanding of the impacts caused by the leading-edge tubercles in a hydraulic turbine, we pretend to apply this device in non-optimized geometries in future studies. Also, we intend to test how other leading-edge tubercles' structural parameters can impact the flow, test how this device can impact if inserted in the turbine splitter, and optimize the tubercles' geometry to achieve its maximum gains in terms of efficiency and torque.

5. ACKNOWLEDGEMENTS

This work has been possible in function of the Conselho Nacional de Desenvolvimento Cientifico e Tecnológico (CNPq), processes 152162/2021-6.

This work has been possible in function of the São Paulo Research Foundation (FAPESP) grants, processes 2019/07947-0 (Regular Process).

We used the test-case provided by NTNU – Norwegian University of Science and Technology under the Francis-99 workshop series.

6. REFERENCES

Abate, G. and Mavris, D.N., 2017. "CFD Analysis of Leading Edge Tubercle Effects on Wind Turbine Performance". In *15th International Energy Conversion Engineering Conference*. AIAA Propulsion and Energy Forum, Atlanta, Geórgia, Estados Unidos da América.

Celebioglu, K., Altintas, B., Aradag, S. and Tascioglu, Y., 2017. "Numerical research of cavitation on Francis turbine runners". *International Journal of Hydrogen Energy*, Vol. 42, No. 28, pp. 17771–17781. URL https://www.sciencedirect.com/science/article/pii/S0360319917312259.

Celik, I., Ghia, U., Roache, P., Freitas, C., Coleman, H. and Raad, P., 2008. "Procedure for Estimation and Reporting of Uncertainty Due to Discretization in CFD Applications". *Journal of Fluids Engineering*, Vol. 130, No. 7. URL https://doi.org/10.1115/1.2960953.

Chen, H.x., Ma, Z., Zhang, W., Zhu, B., Zhang, R., Wei, Q., Zhang, Z.c., Liu, C. and He, J.w., 2017. "On the hydrodynamics of hydraulic machinery and flow control". *Journal of hydrodynamics*, Vol. 29, No. 5, pp. 782–789. URL https://doi.org/10.1016/S1001-6058(16)60789-8.

Dewan, Y., Custer, C. and Ivashchenko, A., 2017. "Simulation of the francis-99 hydro turbine during steady and transient operation". *Journal of Physics: Conference Series*, Vol. 782. URL https://doi.org/10.1088/1742-6596/782/1/012003.

Fish, F.E. and Battle, M.J., 1995. "Hydrodynamic Design of the Humpback Whale Flipper". *Journal of Morphology*, Vol. 225, No. 1, pp. 51–60. URL https://doi.org/10.1002/jmor.1052250105.

Gavrilov, A., Dekterev, A., Minakov, A., Platonov, D. and Sentyabov, A., 2017. "Steady state operation simulation of the Francis-99 turbine by means of advanced turbulence models". *Journal of Physics: Conference Series*, Vol. 782. URL https://doi.org/10.1088/1742-6596/782/1/012006.

Gruber, T., Murray, M.M. and Fredriksson, D.W., 2011. "Effect of Humpback Whale Inspired Tubercles on Marine Tidal Turbine Blades". In *Volume 2: Biomedical and Biotechnology Engineering; Nanoengineering for Medicine and Biology*. ASME, Denver, Colorado, Estados Unidos da América, pp. 851–857. URL https://doi.org/10.1115/IMECE2011-65436.

Johari, H., Henoch, C., Custodio, D. and Levshin, A., 2007. "Effects of Leading-Edge Protuberances on Airfoil Performance". *AIAA Journal*, Vol. 45, No. 11, pp. 2634–2642. URL https://doi.org/10.2514/1.28497.

Kadivar, E., Moctar, O. and Javadi, K., 2018. "Investigation of the effect of cavitation passive control on the dynamics of unsteady cloud cavitation". *Applied Mathematical Modelling*, Vol. 64, p. 333–356. URL https://doi.org/10.1016/j.apm.2018.07.015.

Kadivar, E., Moctar, O. and Javadi, K., 2019. "Stabilization of cloud cavitation instabilities using cylindrical cavitating-bubble generators (ccgs)". *International Journal of Multiphase Flow*, Vol. 115, p. 108–125. URL https://doi.org/10.1016/j.ijmultiphaseflow.2019.03.019.

Liu, C., Yan, Q. and Wood, H.G., 2020. "Numerical investigation of passive cavitation control using a slot on a three-dimensional hydrofoil". *International Journal of Numerical Methods for Heat & Fluid Flow*, Vol. 30, No. 7, pp. 3585–3605. URL https://doi.org/10.1108/HFF-05-2019-0395.

Minakov, A., Platonov, D., Sentyabov, A. and Gavrilov, A., 2017. "Francis-99 turbine numerical flow simulation of steady state operation using RANS and RANS/LES turbulence model". *Journal of Physics: Conference Series*, Vol. 782. URL https://doi.org/10.1088/1742-6596/782/1/012005.

Ministério de Minas e Energia (MME) and Empresa de Pesquisa Energética (EPE), 2020. "Plano Decenal de Expansão de Energia 2029". Technical report, Rio de Janeiro, Rio de Janeiro,Brasil. URL https://www.epe.gov.br/pt/publicacoes-dados-abertos/publicacoes/plano-decenal-de-expansao-de-energia-2029.

Shi, W., Rosli, R., Atlar, M., Norman, R., Wang, D. and Yang, W., 2016. "Hydrodynamic performance evaluation of a tidal turbine with leading-edge tubercles". Elsevier, Vol. 117, pp. 246–253. URL https://doi.org/10.1016/j.oceaneng.2016.03.044.

Trivedi, C., Cervantes, M.J., Gandhi, B.K. and Dahlhaug, O.G., 2013. "Experimental and Numerical Studies for a High Head Francis Turbine at Several Operating Points". *Journal of Fluids Engineering*, Vol. 135, No. 11. URL https://doi.org/10.1115/1.4024805.

Yakhot, A., Orazag, S.A., Thangam, S., Gatski, T.B. and Spezialle, C.G., 1992. "Development of turbulence models for shear flows by a double expansion technique". *Physics of Fluids A: Fluid Dynamics*, Vol. 4, No. 7, pp. 1510–1520. URL https://doi.org/10.1063/1.858424.

Zhang, L., Wang, W. and Guo, Y., 2007. "Intrinsic features of turbulent flow in strongly 3-D skew blade passage of a francis turbine". *Journal of Hydrodynamics, Ser. B*, Vol. 19, No. 1, pp. 92–99. URL https://doi.org/10.1016/S1001-6058(07)60033-X.

Zhang, R.K. and Wu, V.D.J.Z., 2012. "Aerodynamic characteristics of wind turbine blades with a sinusoidal leading edge". *Wind Energy*, Vol. 15, No. 3, pp. 407–424. URL https://doi.org/10.1002/we.479.

Zhang, Y., Guo, Z., Zhu, X., Li, Y., Song, X., Cai, C., Kamada, Y., Maeda, T. and Li, Q., 2022. "Investigation of aerodynamic forces and flow field of an h-type vertical axis wind turbine based on bionic airfoil". *Energy*, Vol. 242, pp. 1–15. doi:https://doi.org/10.1016/j.energy.2021.122999.

7. RESPONSIBILITY NOTICE

The authors are solely responsible for the printed material included in this paper.